

Hard-disk fluid revisit

^{1,2}Hanqing Zhao and ^{1,3}Hong Zhao*

¹*Department of Physics and Institute of Theoretical Physics and Astrophysics,
Xiamen University, Xiamen 361005, Fujian, China*

²*Department of Modern Physics, University of Science and Technology of China, Hefei, 230026, China and*

³*Collaborative Innovation Center of Chemistry for Energy Materials, Xiamen University, Xiamen 361005, China*

(Dated: December 6, 2018)

We study the velocity and energy current autocorrelation functions in hard-disk fluid by large-scale simulations. The t^{-1} long-time tail is reconfirmed for the former while is verified for latter. The validity of several essential hydrodynamics and kinetics predictions are checked with varying the disks density. The significant difference between the two autocorrelation functions are revealed. The long-time tail of the velocity autocorrelation is derived using an intuitive picture, based on which a unified formula of the velocity autocorrelation function is presented. The mechanisms are discussed by studying the relaxation property of the momentum and local current.

PACS numbers: 05.60.Cd, 44.10.+i, 05.45.-a, 05.20.Jj

The hard spheres and hard disks are simplest models of a fluid. The study of such models has general importance for gases since their structures do not differ in any significant way from that corresponding to more complicated interatomic potentials [1]. Though over many decades [1] [2] [3], fundamental problems related to their transport behavior are still remained. On one hand, the traditional kinetic theory [1] [2], predicts that if a system is not in the critical point, in general its autocorrelation functions decay exponentially. On the other hand, the hydrodynamics analysis predicts that these functions in general decay in the power-law manner [1] [6] of $c(t) \sim t^{-d/2}$ at large times even for lattices [22], where d is the dimensionality. Meanwhile, mode coupling theories argue that the power-law tail characterizes intermediate times, while an asymptotic decay as $c(t) \sim (t\sqrt{\ln(t)})^{-1}$ is expected at larger times for $d = 2$ by the self-consistent mode coupling theories [14]. Summering these theoretics we get

$$c(t) = \begin{cases} b_k \exp(-\xi t), t \sim t_0 \\ b_h t^{-\frac{d}{2}}, t \sim P t_0 \\ b_m (t\sqrt{\ln(t)})^{-1}, t \gg t_0 \quad (d = 2) \end{cases}, \quad (1)$$

where t_0 is the mean free time between two successive collisions, b_k , b_h and b_m are constants, P is a large positive constant. Open problems are as follows. (a) How to bridging the kinetic and hydrodynamics representations to get an unified $c(t)$ instead of the piecewise ones. This is important since to calculate the transport coefficient using the Green-Kubo formula one needs a continuous $c(t)$. This goal has just been attacked by a group of researchers but using parameter fitting. (b) Testing theoretical predictions by conclusive numerical simulations. Qualitatively, the $t^{-\frac{d}{2}}$ tail of the velocity autocorrelation function has been repeatedly confirmed [3] [5] [7] [15] [16] since Alder and Wainwright observed this property. Recent accurate simulation studies [15] of hard-disk fluid not only recurs the power-law of t^{-1} perfectly at low densities but also confirm that the logarithmic tail of $(t\sqrt{\ln(t)})^{-1}$ do may appear at moderately densities. For this goal, 10^6 hard disks are applied in their improved event-driven molecular dynamics algorithm. This work however did not discuss the fitness of the amplitude b^h . For the current autocorrelation as well as the viscosity current autocorrelation functions, whether they do show the power-law tail has not been definitely evidenced by direct simulations, though efforts have been done from the early years [8]. (c) At what an extent the long-time tail influences on the observed values of transport coefficients. It is quite surprising, as pointed in Ref. [12], few discussions have focused on this topic. It is usually supposed to be negligible for practical applications [10] [12].

In this Letter, we study the hard-disk fluid at the equilibrium state by large-scale simulations to find partial solutions to above questions. Our studies focus on the velocity autocorrelation $c_v(t) = \langle v_x(0)v_x(t) \rangle$ and the current autocorrelation $c_J(t) = \langle J_x(0)J_x(t) \rangle$, where $v_x(t)$ represents the x-component of the velocity of a tagged particle and $J_x(t)$ is the x-component energy current of the system, and $\langle \cdots \rangle$ represents the ensemble average. We first study $c_v(t)$ to estimate the minimum system size for conclusive simulations beyond which the finite-size effect may be negligible. With the confidence size, the t^{-1} power-law tail is perfectly revealed both for $c_v(t)$ and $c_J(t)$ in the dilute case. The difference between these two autocorrelation functions are shown. We then investigate the probability distribution function $\rho(\mathbf{r}, t)$ of the tagged particle, as well as the relaxation behavior of the momentum and local current initially carried by the tagged particle, manifested by the spatiotemporal correlation functions $c_v(\mathbf{r}, t)$ and $c_j(\mathbf{r}, t)$ respectively. These studies enables us to derive the power-law tail of $c_v(t)$ in an intuitionistic manner, and thus consequently to

construct the unified expression of $c_v(t)$. Meanwhile, we show that the same arguments is not applicable to $c_J(t)$ and its decay behavior need not to be similar to that of $c_v(t)$. Indeed, at moderate densities, while $c_v(t)$ shows a good agreement to the logarithmic tail $(t\sqrt{\ln(t)})^{-1}$ at large times, $c_J(t)$ seems to decay in a way even slower than the t^{-1} manner. We finally discuss the influence of the tail on the observed values of transport coefficients.

To proceed the simulation, we divide the space into 10×10 bins, and put a disk of diameter σ with unit mass in each bin. In this way the particle density in our study is fixed at $n = 0.01$. The event-driven molecular dynamics algorithms with periodic boundary conditions are applied to evolve the system. The disks are set random velocities of $\langle v^2 \rangle / 2 = 1$, which is corresponding to the system temperature of $T = 1$ when the Boltzmann constant k_B is set to be unit. Then adjusting the velocities slightly to make the total momentum to be zero, and evolves the system for a sufficient long time ($> 10^6$) to relax it to the stationary state before the calculation. With $\sigma = 2$, which is corresponding to an area function $\phi = n\pi\sigma^2/4 \approx 0.03$, Fig. 1(a) shows $c_v(t)$ calculated with the $L \times L$ square model at $L = 500, 1000, 2000$, and 3000 respectively. 10^{10} pairs samples of $v_x(0)v_x(t)$ are used for the ensemble average. The finite-size effect manifested by the system-size dependent oscillation is clearly explored. It is known that the effect is first take place around $t \sim L/2v_s$ [15][20][16] when an excited wave at a position meet again in the periodic boundary and induce a valley on $c(t)$ by waves superposition, where $v_s = 1.6$ at $\phi \approx 0.03$ [15]. This kind of finite-size effect has been studied in detail in the 1D diatomic hard-core gas [20], where it is correlated to the configuration recurrence. On the other hand, to fit the power-law tail, the fitting window should be sufficient far from the turning point τ_v which separating the exponential and power-law decay stages. This consideration asks a fitting window of $[2\tau_v, L/2v_s]$. For $c_v(t)$ at this density, $\tau_v \sim 120$ [Fig. 1(a)]. The cases of $L = 500$ and 1000 can not meet the criterion, but at $L \geq 2000$ such a fitting window becomes applicable. Fitting within the windows, we obtain $c_v(t) \sim t^{-1.10}$ and $\sim t^{-1.08}$ for $L = 2000$ and $L = 3000$ respectively. Within numerical errors, the t^{-1} tail is confirmed. Therefore, to confidently identify the tail of $c_v(t)$ at this density, the system size should be $L \geq 2000$. τ_v decreases with the increase of ϕ , so this scale of size is also suitable for high density cases.

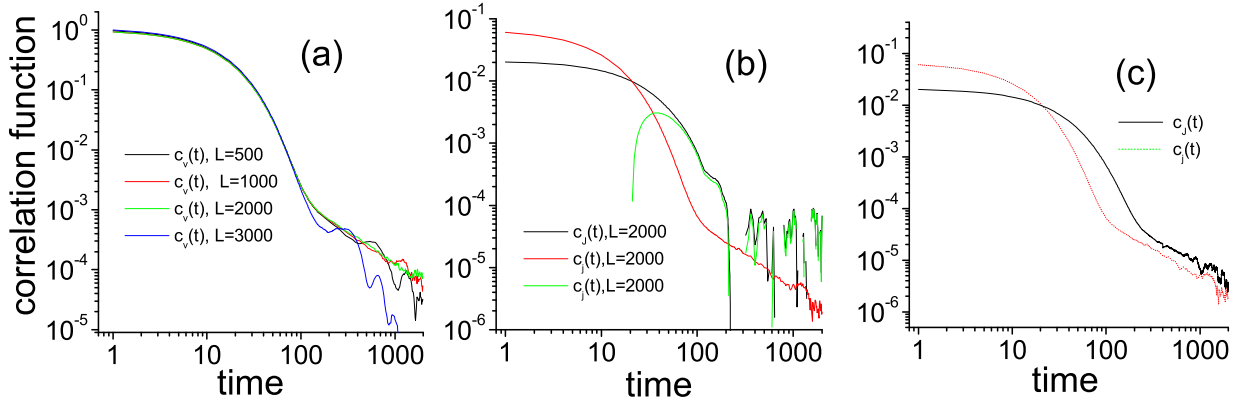


FIG. 1: (Color lines) The autocorrelation functions vis time. (a) The size dependence of the velocity auto correlation function. (b) Local current correlation function (red) and $\bar{c}_j(t)$ (green) calculated using 10^{10} enesml average. The scaled current autocorrelation function (black) is obtained by $c_J(t) = c_j(t) + \bar{c}_j(t)$. (c) The current autocorrelation function (black) obtained with more large-scale simulation. Local current autocorrelation function (red) is from Fig. 1(b).

In calculating $c_v(t)$, since each disk can be considered to move independently, evolving a system to a period t one gets $2N$ samples of $v_x(0)v_x(t)$ since $\langle v_x(0)v_x(t) \rangle = \langle v_y(0)v_y(t) \rangle$. However, the energy current is the sum of local currents of disks, i.e., $\mathbf{J} \equiv \sum_k \mathbf{j}_k$ with $\mathbf{j}_k = v_k^2 \mathbf{v}_k$ representing the local current of the k th disk. Evolving the system to the same period one can only get 2 pairs of $J_x(0)J_x(t)$. Thus, if one wants to calculating $c_J(t)$ using the same amount of samples as in getting $c_v(t)$, N times of the evolution time is needed. This is the main reason why the calculation of $c_J(t)$ is so difficult. Notice that $c_J(t) = \langle \mathbf{J}(0) \cdot \mathbf{J}(t) \rangle / 2 = (N \langle \mathbf{j}_1(0) \cdot \mathbf{j}_1(t) \rangle + N \langle \mathbf{j}_1(0) \cdot \sum_{k \neq 1} \mathbf{j}_k(t) \rangle) / 2 \equiv N(c_j(t) + \bar{c}_j(t))$, $c_J(t)$ thus can be divided into two parts, where the index 1 represents the tagged particle, $c_j(t)$ is the local current autocorrelation of the tagged particle and $\bar{c}_j(t)$ is the correlation of the initial local current of the tagged particle to other particles. In Fig. 1(b), using a square model with $L = 2000$, we show $c_j(t)$ and $\bar{c}_j(t)$ obtained with bath 10^{10} ensemble samples. The curve $c_J(t)/N$ is also shown in the plot. It can be seen that $c_j(t)$ do show the

power-law tail of t^{-1} , though its turning point τ_j is slightly smaller than τ_v . This fact implies that the decay of $c_J(t)$ must slow or equal to t^{-1} law. The reason is that if $\bar{c}_j(t)$ decays faster than $\sim t^{-1}$ asymptotically, then the t^{-1} will be dominant $c_J(t)$ eventually. Otherwise, if $\bar{c}_j(t)$ decays slower than t^{-1} , $c_J(t)$ would be eventually dominated by $\bar{c}_j(t)$ and decay behavior as $\bar{c}_j(t)$ does. If the global $\bar{c}_j(t)$ can be obtained, the exact decay law of $c_J(t)$ can be concreted. However, fluctuations in the tail part of $\bar{c}_j(t)$ is too big. The reason is that in calculating $\bar{c}_j(t)$, the amplitude of initial fluctuations of $\mathbf{j}_1(0) \cdot \sum_{k,k \neq 1} \mathbf{j}_k(0)$ is proportional to $\sqrt{N} \mathbf{j}_1(0) \cdot \mathbf{j}_1(0)$. To suppress the fluctuations to the same level of $c_v(t)$ or $c_j(t)$, one needs N times more samples since statistical errors decay as $1/\sqrt{N}$ with the ensemble number. As a result, the computation complicity of $\bar{c}_j(t)$ is at the same level as in calculating $c_J(t)$.

This fact implies if we spent one day to calculate $c_v(t)$ or $c_j(t)$, then one needs 4×10^4 days to obtain $c_J(t)$. We have to recur to a less accurate manner to approach the goal. Notice that in the equilibrium state the current alone x and y directions have no cross correlation, we apply a rectangle model $L_x \times L_y$ with $L_y = 400$ and $L_x = 3000$ to calculate $c_J(t)$ using current fluctuations alone the x direction only. In this case only 12000 particles are involved in the evolution. Fig. 1(c) shows $c_J(t)$ calculated with 10^9 samples. We have checked that there is no qualitative difference if decreases the width of the rectangle till to $L_y = 200$. Though the tail still shows noticeable fluctuations, a definite conclusion can be drawn – $c_J(t)$ do show a tail of $\sim t^{-1}$ approximately. For a comparison, we replot $c_j(t)$ of Fig. 1(b) in Fig. 1(c). The most important fact is that $\tau_J \gg \tau_j(\tau_v)$.

To understand the underlie mechanism, we turn to study the diffusion behavior of the tagged particle, as well as of the momentum and local current initially carried on the tagged particle. Fig. 2(a) shows the probability distribution function $\rho(\mathbf{r}, t)$ of the tagged particle. It is obtained by tracing the motion of the tagged particle directly. This function can be fitted by a Gaussian function $c(\mathbf{r}, t) = \frac{1}{4\pi Dt} e^{-\frac{\mathbf{r}^2}{4Dt}}$ with $D = 13.4$ (which is calculated using the Enskog formula of diffusion constant [4][12]) at different times (see the sections in the figure), indicating that the tagged particle preforms the Brownian motion.

The diffusion of another two quantities need to be calculated in a different way. Let $\mathbf{A}(0)$ represent a physical quantity carried on the tagged particle at $t = 0$. Picking up a disk to be the tagged particle and setting the initial position of the tagged particle to be the origin, and then dividing a 2000×2000 square into 10×10 bins, we investigate how $\mathbf{A}(0)$ is spreads to the surroundings. Let $\mathbf{A}(\mathbf{r}, t)$ represent the density of the quantity in the bin centering \mathbf{r} . At $t = 0$, nonvanishing correlation $\langle \mathbf{A}(0) \cdot \mathbf{A}(\mathbf{r}, 0) \rangle$ with $\mathbf{r} \neq \mathbf{0}$ should represent the non-causation correlation. This term should be subtracted from the correlation $\langle \mathbf{A}(0) \cdot \mathbf{A}(\mathbf{r}, t) \rangle$ for the purpose of tracing the motion induced by $\mathbf{A}(0)$. This consideration gives [19][20]

$$c_A(\mathbf{r}, t) = \langle \mathbf{A}(0) \cdot \mathbf{A}(\mathbf{r}, t) \rangle / \langle |\mathbf{A}(0)|^2 \rangle + c \quad (2)$$

with $c = -\langle \mathbf{A}(0) \cdot \mathbf{A}(\mathbf{r}, 0) \rangle / \langle |\mathbf{A}(0)|^2 \rangle$. Because of the homogeneity of the system, c is a constant independent on \mathbf{r} . For conserved quantity such as the momentum, it has $\sum_{i=1}^N m \mathbf{v}_i = 0$ and one derives $c = 1/N_c$ [?], where N_c is the number of bins. For other quantity, this constant needs to be determined numerically.

Fig. 2(b)-2(c) show $c_v(\mathbf{r}, t)$ with $\mathbf{A} = \mathbf{v}$ and $c_j(\mathbf{r}, t)$ with $\mathbf{A} = \mathbf{j}$ respectively, where \mathbf{v} and \mathbf{j} are the velocity and local current of the tagged particle initially. Since the mass of disks is set to be unity, \mathbf{v} is identical to the momentum and thus $c = 1/N_c$. For the local current, we obtain $c \approx 2/3N_c$ by numerical simulations, which implies that $c_j(\mathbf{r}, t)$ is also restricted by certain hidden conservation law. Fig. 2 indicates that the momentum and local current relax in the similar way. Both appear as a center peak surrounded by a ring peak. The section plots further show that the center peaks can be fitted by $c_v^c(\mathbf{r}, t) = \frac{a_v}{4\pi D_v t} e^{-\frac{\mathbf{r}^2}{4D_v t}}$ and $c_j^c(\mathbf{r}, t) = \frac{a_j}{4\pi D_j t} e^{-\frac{\mathbf{r}^2}{4D_j t}}$ respectively with $D_v = D_j = 14.1$, and $a_v = 1/2$ and $a_j = 1/3$. The momentum diffusion constant is related to the viscosity coefficient η as $D_v = \eta/nm$. The value of D_v is also calculated following the Enskog formula [4][12]. These center peaks can be identified to be the heat mode predicted by the linearized hydrodynamics [1]. The ring peak spreads outwards with sound velocity v_s and thus may be identified as the sound mode.

The relaxation process of these two quantities thus becomes clear. The quantity $\mathbf{A}(0)$ initially carried on the tagged particle evolves into two parts. One part performs the Brownian motion as the heat mode. Another part moves outwards ballistically as the sound mode. As a result, the constants a_v and a_j measure the rates that the initial momentum and local current are remained in the center peaks correspondingly. In deed, $c_v(\mathbf{r}, t)$ is similar [Fig. 2(d)] even quantitatively to the spatiotemporal correlation function of mass-density fluctuations that defines the so-called dynamics structural factor or the van Hove function. It is known that Landau–Placzek ratio, the rate of the volume of the heat-mode peak to that of the sound-mode peak, is equal to $C_P/C_v - 1 = \gamma - 1$, where C_P and C_v are specific heat at constant pressure and volume respectively[1]. Assuming that a_v measures the rate of the heat mode to the sound mode, and we thus get $a_v = 1/\gamma$.

Based on these observations we can calculate the tails of $c_v(t)$ and $c_j(t)$. Lets take $c_v(t)$ as an example. Initially the tagged particle transport its momentum to surroundings by collisions. Then part of the momentum is spread

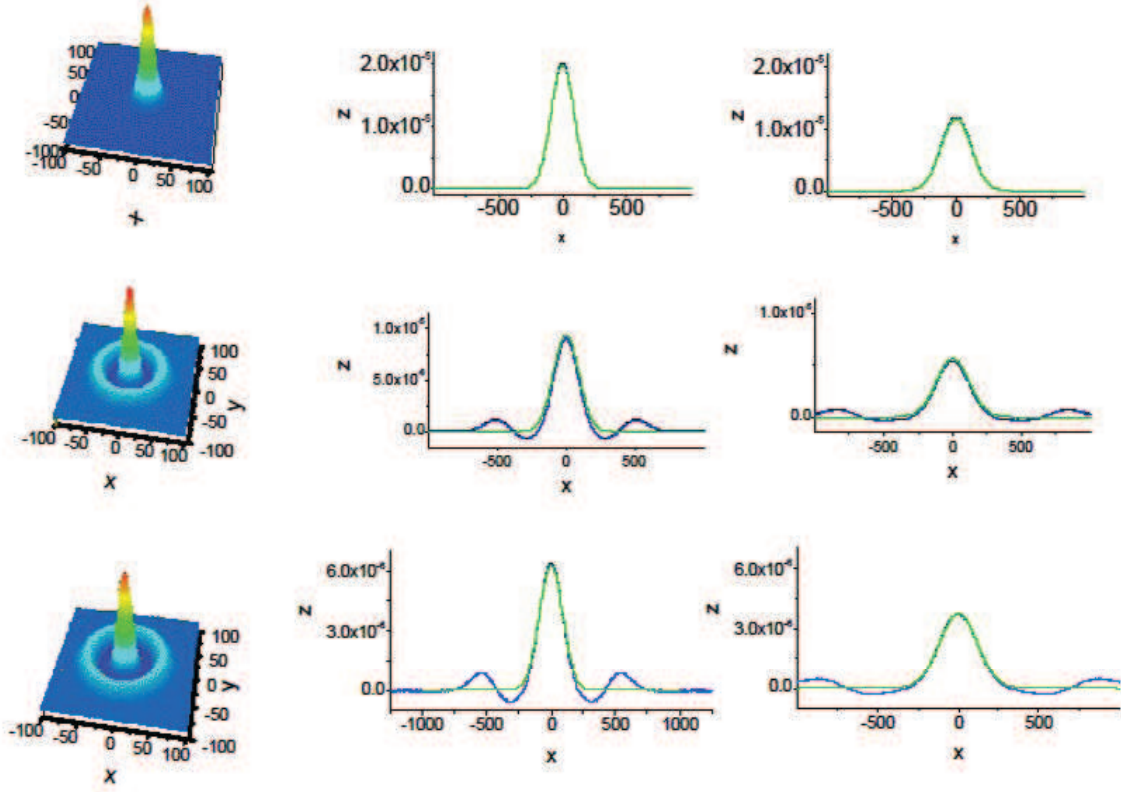


FIG. 2: Plots of the Lennard-Jones potential function (a) and its asymmetry degree (b) at various parameter sets. From top to bottom in (a) but reversely in (b), the curves are for $(m, n) = (12, 6)$, $(8, 4)$, $(6, 3)$, $(4, 2)$, and $(2, 1)$, respectively.

out by the sound mode, and the rest performs the diffusive motion. The latter part may feedback to the tagged particle by correlated collisions. Quantitatively, the tagged particle has the probability $\rho(\mathbf{r}, t)$ at the unit volume centering \mathbf{r} , in which there are $1/n$ particles and each of them takes an amount $\langle v^2(0) \rangle c_v(\mathbf{r}, t)/n$ of $\langle v^2(0) \rangle$ in average, where $\langle v^2(0) \rangle = \frac{k_B T}{M}$. The average feedback momentum to the tagged particle thus can be calculated by $c_v^h(t) = (1/n)(\frac{k_B T}{M}) \int_0^\infty c_v(\mathbf{r}, t) \rho(\mathbf{r}, t) d\mathbf{r}$. Since $\rho(\mathbf{r}, t)$ is a Gaussian function which decays to sufficiently small values in the region of the ring peak, we can use $c_v^c(\mathbf{r}, t) = \frac{a_v}{4\pi D_v t} e^{-\frac{r^2}{4D_v t}}$ to replace $c_v(\mathbf{r}, t)$. With this simplification, we obtain

$$c_v^h(t) = \frac{a_v}{4\pi(D + D_v)n} \left(\frac{k_B T}{M} \right) t^{-1}. \quad (3)$$

For disks it has $\gamma = 2$ and thus $a_v = 1/2$ if neglect the effect of disk volumes. This formulas is identical to those derived based on the hydrodynamically arguments and the high-order kinetic theory[1][6, 13]

The eq. (3) is incorrect in the kinetic stage. In this stage the tagged particle loses its initial momentum with the rate $(1 - e^{-\frac{k_B T}{m D_v t}})$. We assume that the lost momentum is also divided into heat mode and sound mode following the rate of a_v , which gives the correction of eq. (3)

$$c_v^h(t) = \frac{a_v}{4\pi(D + D_v)n} \left(\frac{k_B T}{M} \right) (1 - e^{-\frac{k_B T}{m D_v t}}) t^{-1}. \quad (4)$$

As a result, we get the unified function

$$c_v(t) = c_v^k(t) + c_v^h(t), \quad (5)$$

where $c_v^k(t) = \frac{k_B T}{M} \exp(-\frac{k_B T}{MD}t)$ is predicted by the kinetic theory representing the direct loss of the moment initially carried on the tagged particle.

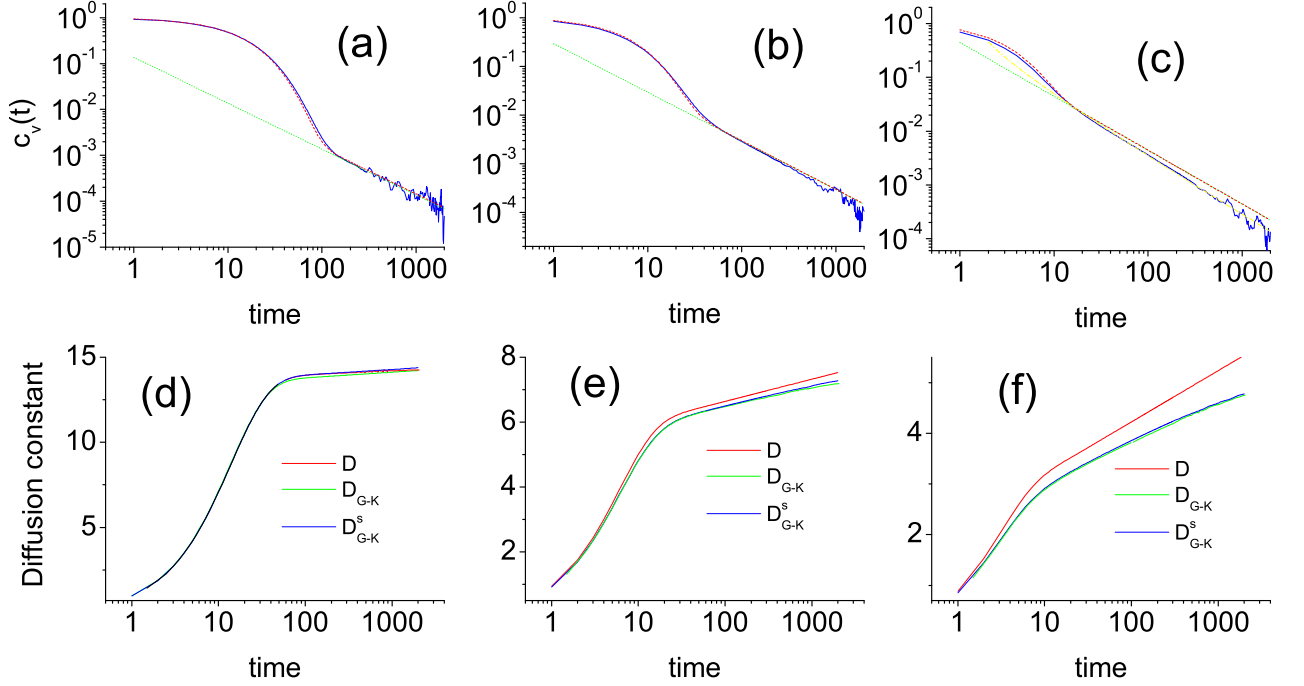


FIG. 3: (Color lines) $c_v(t)$ at $\phi = 0.03$ (a), 0.13 (b) and 0.28 (c). The dot lines are following eq. (3), the dashed lines are following eq. (5). The dot-dashed line in (c) is the logarithmic fitting. (d)-(f) show $D(t)$ (green) obtained by direct tracing the tagged particle, $D_{G-K}^s(t)$ (blue) obtained by directly use of $c_v(t)$ of simulation, and $D_{G-K}(t)$ (red) obtained by eq. (5). The densities are as Fig. 3(a)-(c) correspondingly.

In Fig 3(a)-(c) we show $c_v(t)$ at densities $\phi = 0.03(\sigma = 2)$, $0.13(\sigma = 4)$ and $0.28(\sigma = 6)$ correspondingly. D and $D_v = \eta/nm$ are calculated following the Enskog formulas. The dot lines are obtained by eq. (3), and the dashed lines obtained by eq. (5), correspondingly. One can see that eq. (3) fits the tails while eq. (5) fits $c_v(t)$ well globally at low densities. The eq. (3) and (5) predict the same tails. At $\phi = 0.28$, remarkable difference appears. The slope of the tail becomes slightly faster than t^{-1} . Applying $c_v(t) = b_m(t\sqrt{\ln(t)})^{-1}$ to fit the tail, the tail can be fitted perfectly.

The valid of eq. (5) implies that the diffusive motion is not exactly as Brownian motion. Insert (5) into the Green-Kubo formula $D_{G-K} = \lim_{\tau \rightarrow \infty} \frac{1}{\tau} \int_0^\tau c_v(t) dt$ one obtains $D_{G-K} = \frac{k_B T}{M} \int_0^\tau e^{-\frac{k_B T}{MD}\tau} d\tau + \frac{a_v}{4\pi(D+D_v)n}(\frac{k_B T}{M})[ln(t) - \int_0^t \tau^{-1} e^{-\frac{k_B T}{MD}\tau} d\tau]$. D_{G-K} predicted by this formula are shown in Fig.3 (d)-(f). On the other hand, the diffusion constant can also be calculated by directly trace the tagged particle, i.e., $\frac{d}{dt}\langle r^2(t) \rangle = D(t)$. Results obtained in this way are also shown in Fig 2(d)-(f). Meanwhile, D_{G-K}^s , representing the result directly calculated using the simulation result of $c_v(t)$, is plotted, too. The curves $D(t)$ and D_{G-K}^s overlap with each other always, indicating that the Green-Kubo formula based on equilibrium time-correlation functions do give the diffusion constant of the tagged particle. At $\phi = 0.03$, they fit with D_{G-K} also, while the deviation appears at $\phi = 0.13$ and becomes remarkable at $\phi = 0.28$. The deviation is induced by the deviation of the tail from the t^{-1} law.

Therefore, exactly particles in the gas preforms the superdiffusive motion with the diffusion constant increase as a function of time. In Table I the diffusion constant D_0 and D_E are obtained by the Boltzmann and Enskog formula respectively [12], D_{G-K}^τ is calculated by truncating the integral at $t = \tau_v$, t_{10} and t_{100} represent the truncation time above which D_{G-K} exceeds 10% and 100% of D_{G-K}^τ . In dilute case of $\phi \sim 0.03$, the deviation of D_{G-K}^τ from D_0 is about 1%, and D_E is about 4%. The hydrodynamics tail correction approaches 10% till $t_{10} = 10^5$. A system of size $L \sim t_{10} v_s \sim 1.6 \times 10^5$ is needed to guarantee the free diffusion of the particle within such a time. In our disk model, there are $L/10$ disks in average alone the moving direction, which gives $L \sim 10^{-5}m$ with this reference that

the average distance between particles in the air is $\sim 3 \times 10^{-9}$ m. The contribution exceeds 20% around $t \sim 10^9$ which is corresponding to $L \sim 0.1$ m. The contribution exceeds 100% till $t \sim 10^{35}$. Therefore, the hydrodynamics contribution is rough negligible in dilute gas within 20% errors. With the increase of the density, as the Table shows that this contribution may become dominant for large systems.

The above discussion can be applied to $c_j(t)$ directly. However, it can not be applied to $c_J(t)$ since the property of $\bar{c}_j(t)$ has not been revealed. As a non-monotonic function, $\bar{c}_j(t)$ may change the profile of $c_j(t)$ and postpone the turning point when adding them together. Indeed, since $c_J(t) = N \int_0^\infty c_j(\mathbf{r}, t) d\mathbf{r}$, the relaxation behavior of $c_J(t)$ is determined not only the center peak but also the ring peak of $c_j(\mathbf{r}, t)$. Therefore, the mechanism of the tail should be different from that of $c_v(t)$. As a result, we have not derive the tail of $c_J(t)$ in the above manner. The tail of $c_J(t)$ has obtained in certain previous works [6]. It reads, $c_J(t)/c_J(0) \sim (2\pi(\eta/m + \kappa/2k_B))^{-1} t^{-1}$, where κ is the thermal conductivity. Unlike the tail of $c_v(t)$, this formula has never been tested by direct simulations since $c_J(t)$ has not been obtained by simulations. Applying the values of η and κ from the Enskog formulas, in Fig. 4(a) we plot $c_J(t)$ predicted by this expression as well as $c_J(t)$ obtained in Fig. 1(c). It seems that the prediction is applicable at this density. However, with the increase of the density, it becomes invalid, as Fig. 4(b)-(c) show. From Fig. 4(b) and (c), the relation $\tau_J \gg \tau_j(\tau_v)$ holds, while another exponential decay stage appears on $c_J(t)$ before the power-law tail. These features can be explained as that $\bar{c}_j(t)$ plays a more significant role at high densities. Indeed, one may notice that the predicted tail crosses over $c_J(t)$ around the end of the first exponential decay stage. Therefore, the invalidation of the theoretical prediction should be related to the multistage behavior of $c_J(t)$ induced by $\bar{c}_j(t)$. Besides, the slopes of tails seems to become slightly slow than t^{-1} .

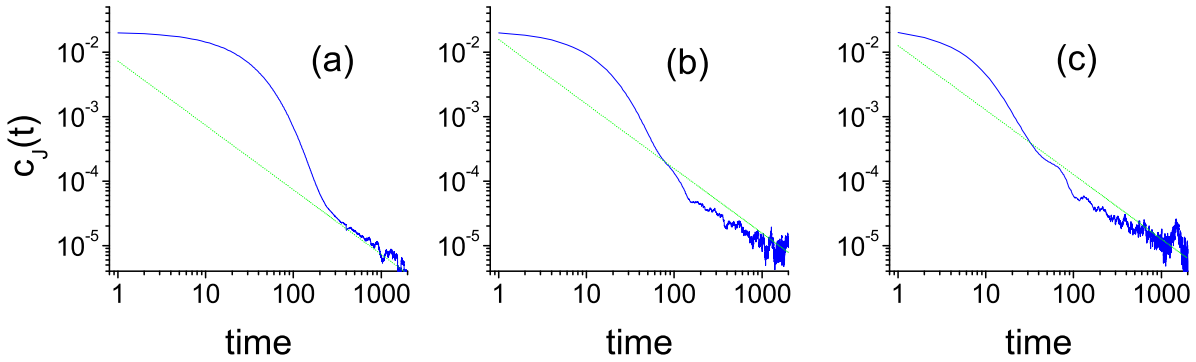


FIG. 4: (Color lines) $c_J(t)$ at $\phi \sim 0.03$ (a), 0.13 (b) and 0.28 (c). The dot lines are obtained following the theoretical predictions.

The thermal conductivity can be calculated by the Green-Kubo formula, $\kappa_{G-K} = \lim_{\tau \rightarrow \infty} \lim_{L \rightarrow \infty} \frac{1}{k_B T^2 V} \int_0^\tau c_J(t) dt$, where V is the volume of the system. Table I shows the results by extrapolating the tail of t^{-1} to the infinite time. It can be seen that the correction from the tail is much smaller than in the case of $D_{G-K}^{\tau_v}$. Even at $\phi \sim 0.28$, the contribution approaches 100% of $\kappa_{G-K}^{\tau_J}$ till $t_{100} = 10^{10}$. The $\kappa_{G-K}^{\tau_J}$ can thus roughly describe the thermal conductivity practically. The deviation of $\kappa_{G-K}^{\tau_J}$ from κ_0 is about 3%, and κ_E is about 2%, in the dilute case. With the increase of the density, it seems that $\kappa_{G-K}^{\tau_J}$ is closer to the Boltzmann formula than to the Enskog formula. Therefore, we can not judge which formula is more precision for thermal conductivity. The multi-stage effect we find above seems not been involved in deriving even the Enskog formula.

Table I Comparisons between kinetic predictions and Green-Kubo formula

ϕ	D_0	D_E	$D_{G-K}^{\tau_v}$	τ_v	t_{10}	t_{100}	κ_0	κ_E	$\kappa_{G-K}^{\tau_J}$	τ_J	t_{10}	t_{100}
0.03	14.10	13.42	13.96	110	10^5	10^{35}	0.564	0.592	0.580	280	10^5	10^{39}
0.13	7.05	5.71	6.40	40	200	10^9	0.282	0.354	0.258	160	6000	10^{16}
0.28	4.70	2.76	2.85	10	16	1000	0.188	0.360	0.139	110	1000	10^{10}

In summary, for the problem (a) we obtain the unified $c_v(t)$ without using any fit parameter. This result applicable to densities up to $\phi \sim 0.1$. At moderately densities the t^{-1} tail is replaced by the logarithmic tail of $(t\sqrt{\ln(t)})^{-1}$. For the problem (b) we confirm that the predicted amplitude b_h is correct for velocity autocorrelation $c_v(t)$ up to $\phi \sim 0.1$. At higher density, the tail becomes logarithmic. The predicted b_h is still useful since the line $b_h t^{-1}$ just cross $c_v(t)$

around the turning point. In the case of energy current autocorrelation $c_J(t)$, we show that $c_J(t) = N(c_j(t) + \bar{c}_j(t))$. The first part is the local current autocorrelation of the tagged particle. It behaves as $c_v(t)$, implies that the decay of the tail of $c_J(t)$ can not faster than that of $c_v(t)$. Direct calculation of $c_J(t)$ confirms that it do decay in the power-law manner of $b_h t^{-1}$ at the dilute density $\phi \sim 0.03$. The amplitude b_h agrees with previous theoretical predictions. However, with the increase of the density, the decay of the tail becomes slower than t^{-1} , and the amplitude diverges from the prediction significantly. We attribute the reason to not involving the multistage decay phenomenon observed in our study in previous theoretical analysis. For the question (c) we show that the diffusion constant of the tagged particle increase as a function of time and it overlaps to that calculated based on the Green-Kubo formula using the simulated $c_v(t)$, indicating that this formula based on linear response theory do can describe the diffusion of the tagged particle. In low-density case of $\phi \sim 0.03$, the hydrodynamic corrections is within 20% up to the macroscopic level. But the contribution may become dominant if further increase the density. In the case of the thermal conductivity, the correction from the tail is much smaller than in the case of diffusion constant. Even at the moderated density, the contribution approaches 100% of κ_{G-K}^T till $t_{100} = 10^{10}$, and thus κ_{G-K}^T can roughly describe the thermal conductivity practically. This is a consequence of $\tau_J \gg \tau_v$. However, the theoretical predictions of either the Boltzmann and Enskog formulas have significant divergence from κ_{G-K}^T .

By studying the spatiotemporal correlation functions $c_v(\mathbf{r}, t)$ and $c_j(\mathbf{r}, t)$ we show that the momentum and local current initially carried by the tagged particle are respectively divided into two parts after a transient period, one part is spread out by the sound mode while the another part is carried by the heat mode. The heat mode performs the normal diffusive motion as the tagged particle does. These facts enable us to derive the formula of the power-law tail of $c_v(t)$ with a simple physical picture, which agrees with that obtained by rigid analysis. The prediction is confirmed by simulations. Furthermore, a formula manifesting $c_v(t)$ from short time to long time region is constructed, which bridges the gap between the kinetic and hydrodynamic descriptions. It is also tested with high precision. The underlying assumption is that either the kinetic and hydrodynamics mechanisms play roles in the whole process of relaxation. This is different from the conventional treatment by separating the process into continuous stages.

There are big differences between $c_J(t)$ and $c_v(t)$. Besides $\tau_J \gg \tau_v$, $c_J(t)$ shows multistage processes at high densities. The reason is that $c_J(t)$ is composited by two parts, $c_j(t)$ and $\bar{c}_j(t)$. The overlap of $\bar{c}_j(t)$ with $c_j(t)$ postpones the turning point and results the multistage decay. In addition, the mechanism resulting the tail of $c_v(t)$ is not applicable to that of $c_J(t)$, in which case just the center peak of $c_j(\mathbf{r}, t)$ play a role. While $c_J(t)$ is just the volume of $c_j(\mathbf{r}, t)$, involving both the center peak and the ring peak. Therefore, $c_J(t)$ and $c_v(t)$ should have different mechanism.

Our studies are stopped around the density of $\phi \sim 0.28$ that is still in the gas phase. At this density, one can already seen the divergence from the linearized hydrodynamics. High density disks fluid should be another topic of further studies.

This work is supported by the NNSF (Grants No. 11335006) of China.

* Electronic address: zhaoh@xmu.edu.cn

- [1] J. P. Hansen and I. R. McDonald, *Theory of Simple Liquids*, 3rd ed. (Academic, London, 2006).
- [2] P. Reusibois and M. de Leener, *Classical Kinetic Theory of Fluids* Wiley-Interscience, New York, 1977.
- [3] B. S. Alder and T. E. Wainwright, Phys. Rev. Lett. 18, 988 (1969), B. J. Alder and T. E. Wainwright, Phys. Rev. A 1, 18 (1970); B. J. Alder, D. M. Gass, and T. E. Wainwright, J. Chem. Phys. 53, 3813(1970).
- [4] D. M. Gass, J. Chem. Phys. 54, 1898(1971)
- [5] J. J. Erpenbeck and W. W. Wood, Phys. Rev. A 26, 1648 1982; J. J. Erpenbeck and W. W. Wood, Phys. Rev. A 32 412(1985)
- [6] B. S. Alder and T. E. Wainwright, Phys. Rev. Lett. 18, 988 (1969), S. R. Dorfman and E. G. D. Cohen, PRL 25, 1257(1970); M. H. Ernst, E. H. Hauge, and J. M. J. van Leeuwen, Phys. Rev. Lett. 25, 1254 (1970); M. H. Ernst, E. H. Hauge, and J. M. J. van Leeuwen, Phys. Rev. A 4, 2055 (1971). J. R. Dorfman and E. G. D. Cohen, Phys. Rev. A 6, 776 (1972).
- [7] J. J. Erpenbeck and W. W. Wood, Phys. Rev. A 26, 1648(1982); J. J. Erpenbeck and W. W. Wood, Phys. Rev. A 32, 412 (1985).
- [8] T. E. Wainwright, B. J. Alder, and D. M. Gass, Phys. Rev. A4, 233(1971).
- [9] J. J. Erpenbeck, and W. W. Wood, Phys. Rev. A 43, 42549(1991)
- [10] S. Viscardy and P. Gaspard, Phys. Rev. E 68, 041204(2003)
- [11] J. W. Dufty, Mol. Phys. 100, 2331 2002 ; J. W. Dufty and M. H. Ernst, ibid. 102, 2123(2004) .
- [12] Ramou Garciu-Rojo, Stefan Luding, J. Javier Brey, Phys. Rev. E 74, 061305(2006)
- [13] Y. Pomeau and P. Reuibois, Physics Reports, 19, 63(1975).
- [14] D. Forster, D. R. Nelson, and M. J. Stephen, Phys. Rev. A 16 732 (1977).

- [15] Masaharu Isobe, Phys. Rev. E 77, 021201(2008)
- [16] S. Bellissima, M. Neumann, E. Guarini, U. Bafle and F. Barocchi1, Phys. Rev. E 92, 042166(2015)
- [17] S. Bellissima, M. Neumann, E. Guarini, U. Bafle, and F. Barocchi1, PHYSICAL REVIEW E 92, 042166 (2015)
- [18] R. Kubo, M. Toda and N. Hashitsume, *Statistical Physics II: Nonequilibrium Statistical Mechanics* (Springer, New York, 1991); D. Andrieux and P. Gaspard, J. Stat. Mech. P02006 (2007).
- [19] H. Zhao, Phys. Rev. Lett. 96, 140602 (2006).
- [20] Shunda Chen, Yong Zhang, Jiao Wang, and Hong Zhao, Phys. Rev. E 87, 032153 (2013)
- [21] F. Bonetto, J. L. Lebowitz, L. Rey-Bellet, *Fourie's Law: A Challenge to Theorists*, Mathematical Physics 2000 (Imperial College Press, London, 2000).
- [22] S. Lepri, R. Livi, A. Politi, Physics Reports **377**, 1 (2003); A. Dhar, Adv. Phys. **57**, 457 (2008).